THE EUROPEAN
PHYSICAL JOURNAL PLUS

Regular Article

Analytical solution of magneto-hydrodynamics with acceleration effects of Bjorken expansion in heavy-ion collisions

A. F. Kord[1,a] [iD]**, A. Ghaani**[1]**, M. Haddadi Moghaddam**[2]

[1] Department of Physics, Hakim Sabzevari University (HSU), P.O. Box 397, Sabzevar, Iran
[2] Department of Physics, University of Turin and INFN, Turin, Via P. Giuria 1, 10125 Turin, Italy

Abstract In this article, we aim to study, in an analytical manner, the $1 + 1$ longitudinal acceleration expansion of hot and dense quark matter as a conducting relativistic fluid with the electric conductivity σ. To this end, the plasma is inserted in the presence of electric and magnetic fields, which are perpendicular together in the transverse plane. To be more realistic, we generalize the Bjorken solution, which includes the acceleration effects on the fluid expansion. We then apply a perturbation fashion in the initial condition to solve the relativistic magneto-hydrodynamics equations. This procedure leads us to achieve the exact algebraic expressions for both electric and magnetic fields. In the process, we also find the effects of the electromagnetic fields on the fluid's acceleration and the energy density correction obtained from the magneto-hydrodynamics solutions.

1 Introduction

It has been demonstrated that a new form of hot and dense nuclear matter is created in the relativistic heavy-ions collisions, which is commonly known as quark-gluon plasma (QGP) [1]. It has also been shown that, during these collisions, strong electromagnetic (EM) fields are generated due to the relativistic motion of the colliding heavy- ions carrying significant positive electric charges. Recently, some investigations have been carried out, in a typical non-central collision such as Pb–Pb at the center of mass energy $\sqrt{s} = 2.76$ TeV and Au–Au at the center of mass energy $\sqrt{s} = 200$ GeV, which have demonstrated that an extremely strong magnetic field is created of the order $10^{18} - 10^{19}$ G, which corresponds to $|eB| \simeq 1$ GeV^2 and is 10^{13} times larger than the effective steady magnetic field which is found in the laboratory [2–6].

It has been argued that the existence of these strong fields is essential for a wide variety of new phenomena such as Chiral Magnetic Effect (CME), Chiral Magnetic wave (CMW), Chiral Electric Separation Effect (CESE), Chiral Hall Separation Effect (CHSE), pressure anisotropy in QGP, influence on the direct and elliptic flow and shift of the critical temperature. Concerning this, some relevant references and review articles are found in Refs. [7–18].

[a] e-mail: a.f.kord@hsu.ac.ir (corresponding author)

On the other hand, some studies have been conducted on the space-time evolution of electromagnetic fields created by the colliding charged beams moving at relativistic speed in the z-direction, as a solution of the Maxwell equations [5,6,19–22]. Additionally, a series of preliminary results have been obtained by estimating the significance of strong EM fields on the QGP medium [3,23–26]. Moreover, some attempts have been made to solve the equations of relativistic magneto-hydrodynamics (RMHD) [4,27–31]. Lately, relativistic magneto-hydrodynamics with longitudinal boost invariance in the presence of finite electric conductivity has also been studied in such works as [32,33].

One of the renowned pictures which describe the expanding of QGP in the beam direction with the exact solution belongs to the boost-invariant (rapidity-independent) Bjorken picture. This solution predicts a flat rapidity distribution of final particles, which is at variance with observations at RHIC, except for a restricted region around mid-rapidity [34,35]. In realistic collisions, boost invariance is violated, and a model should be investigated that is more faithful and not far from the accelerationless Bjorken picture. There have been several attempts to generalize the Bjorken model, such as [36]. Some have included accelerating solutions of relativistic fluid dynamics to obtain the more realistic estimation [37].

In the present work, we are going to investigate the response of resistive fluid with finite electrical conductivity σ to the presence of coupled transverse electric and magnetic fields in an analytical manner. Here, we consider the combination of relativistic hydrodynamic equations with Maxwell's equations and solve in 1 + 1 dimensions a set of coupled RMHD equations. Building upon previous studies, we assume that a magnetic field is produced in the y direction, which is perpendicular to the reaction plane, and that the electric field is created in a reaction plane in the x direction. We consider the QGP medium to be created quickly after collisions with the generalized Bjorken longitudinal expansion. We are interested in obtaining solutions that represent the resistive relativistic magneto-hydrodynamic (RRMHD) extension of the one-dimensional generalized Bjorken flow ($v_z \neq \frac{z}{t}$) along the z direction, with the Lorentz force being directed along the x direction.

The presentation of our analysis in this piece is structured as follows: In the next section, we will introduce the RRMHD equations in their most general form, considering them in plasma with finite electrical conductivity. In Sect. 3, we will go on to solve the RRMHD equations with a perturbative approach and obtain the analytic solution for the EM fields and the energy density. The discussion on the results and the properties of EM fields, energy density, and acceleration parameter will be what constitutes in Sect. 4. Finally, the last section is devoted to some concluding remarks.

2 Resistive relativistic magneto-hydrodynamic

To describe the interaction of matter and electromagnetic fields in quark-gluon plasma, we can resort to the RMHD framework [27,38,39]. For the sake of simplicity, we assume an ideal ultra-relativistic plasma with massless particles and finite electrical conductivity σ. Thus, in the equation of state, the pressure is merely proportional to the energy density: $P = \kappa\epsilon$ where κ is constant. For an ideal fluid with finite electrical conductivity, which is called resistive fluid, equations of RRMHD can be written in the form of covariant conservation laws:

$$d_\mu T_{\text{matter}}^{\mu\nu} = -J_\lambda F^{\lambda\nu} \tag{1}$$

$$d_\mu F^{\star\mu\nu} = 0 \tag{2}$$

$$d_\mu F^{\mu\nu} = -J^\nu, \qquad d_\mu J^\mu = 0 \tag{3}$$

The energy-momentum tensor for the fluid is:

$$T^{\mu\nu}_{\text{matter}} = (\epsilon + P)u^\mu u^\nu + Pg^{\mu\nu}, \qquad P = \kappa\epsilon \tag{4}$$

where u^μ, ϵ, and P stand, respectively, for fluid four-velocity, energy density, and pressure. The metric tensor at flat space-time is $g_{\mu\nu} = diag(-, +, +, +)$, and the fluid four-velocity ($u_\mu u^\mu = -1$) is defined as:

$$u^\mu = \gamma(1, \mathbf{v}), \qquad \gamma = \frac{1}{\sqrt{1 - v^2}}$$

Also, tensors of the electromagnetic fields and current density are given by:

$$F^{\mu\nu} = u^\mu e^\nu - u^\nu e^\mu + \epsilon^{\mu\nu\lambda\kappa}b_\lambda u_\kappa \tag{5}$$

$$F^{\star\mu\nu} = u^\mu b^\nu - u^\nu b^\mu - \epsilon^{\mu\nu\lambda\kappa}e_\lambda u_\kappa \tag{6}$$

$$J^\mu = \sigma e^\mu \tag{7}$$

Here $\epsilon^{\mu\nu\lambda\kappa} = (-g)^{-1/2}[\mu\nu\lambda\kappa]$ is the Levi-Civita tensor density with $g = \det\{g_{\mu\nu}\}$ and $[\mu\nu\lambda\kappa]$ is the completely antisymmetric Levi-Civita symbol. Besides:

$$e^\mu = F^{\mu\nu}u_\nu, \qquad b^\mu = F^{\star\mu\nu}u_\nu, \qquad e^\mu u_\mu = b^\mu u_\mu = 0 \tag{8}$$

e^μ and b^μ are electric and magnetic field four-vector in the local rest frame of the fluid, which is related to the one measured in the lab frame.

In Eqs. (1) to (3) the covariant derivatives are given by:

$$d_\mu A^\nu = \partial_\mu A^\nu + \Gamma^\nu_{\mu m}A^m \tag{9}$$

$$d_p A^{\mu\nu} = \partial_p A^{\mu\nu} + \Gamma^\mu_{pm}A^{m\nu} + \Gamma^\nu_{pm}A^{\mu m} \tag{10}$$

where Γ^i_{jk} are the Christoffel symbols:

$$\Gamma^i_{jk} = \frac{1}{2}g^{im}\left(\frac{\partial g_{mj}}{\partial x^k} + \frac{\partial g_{mk}}{\partial x^j} - \frac{\partial g_{jk}}{\partial x^m}\right) \tag{11}$$

It is more convenient to work with Milne coordinates than with the standard Cartesian coordinates for a longitudinal boost invariant flow:

$$(\tau, x, y, \eta) = \left(\sqrt{t^2 - z^2}, x, y, \frac{1}{2}ln\frac{t + z}{t - z}\right) \tag{12}$$

Here, the metric is presented as:

$$g^{\mu\nu} = diag\left(-1, 1, 1, \frac{1}{\tau^2}\right), \qquad g_{\mu\nu} = diag(-1, 1, 1, \tau^2) \tag{13}$$

By executing the projection of Eq. (1) along the longitudinal and transverse direction concerning u^μ, the conservation equations can be rewritten:

$$u_\nu(d_\mu T^{\mu\nu}_{\text{matter}} = -J_\lambda F^{\lambda\nu}) \rightarrow D\epsilon + (\epsilon + P)\Theta = e^\lambda J_\lambda \tag{14}$$

$$\Delta_{\alpha\nu}(d_\mu T^{\mu\nu}_{\text{matter}} = -J_\lambda F^{\lambda\nu}) \rightarrow (\epsilon + P)Du_\alpha + \nabla_\alpha P = g_{\alpha\nu}F^{\nu\lambda}J_\lambda - u_\alpha e^\lambda J_\lambda \tag{15}$$

where:

$$D = u^\mu d_\mu, \quad \Theta = d_\mu u^\mu, \quad \Delta_{\alpha\nu} = g_{\alpha\nu} + u_\alpha u_\nu, \quad \nabla^\mu = d^\mu + u^\mu D \tag{16}$$

In contrast with the energy-momentum tensor $T^{\mu\nu}$, the dual electromagnetic tensor $F^{*\mu\nu}$ is anti-symmetric; hence the homogeneous Maxwell's equation, $d_\mu F^{*\mu\nu} = 0$, leads to the following equations:

$$\partial_x F^{*x\tau} + \partial_y F^{*y\tau} + \partial_\eta F^{*\eta\tau} = 0 \tag{17}$$

$$\partial_\tau F^{*\tau x} + \partial_y F^{*yx} + \partial_\eta F^{*\eta x} + \frac{1}{\tau} F^{*\tau x} = 0 \tag{18}$$

$$\partial_\tau F^{*\tau y} + \partial_x F^{*xy} + \partial_\eta F^{*\eta y} + \frac{1}{\tau} F^{*\tau y} = 0 \tag{19}$$

$$\partial_\tau F^{*\tau\eta} + \partial_x F^{*x\eta} + \partial_y F^{*y\eta} + \frac{1}{\tau} F^{*\tau\eta} = 0 \tag{20}$$

Also, the in-homogeneous Maxwell's equations ($d_\mu F^{\mu\nu} = -J^\nu$) are given by:

$$\partial_x F^{x\tau} + \partial_y F^{y\tau} + \partial_\eta F^{\eta\tau} = -J^\tau \tag{21}$$

$$\partial_\tau F^{\tau x} + \partial_y F^{yx} + \partial_\eta F^{\eta x} + \frac{1}{\tau} F^{\tau x} = -J^x \tag{22}$$

$$\partial_\tau F^{\tau y} + \partial_x F^{xy} + \partial_\eta F^{\eta y} + \frac{1}{\tau} F^{\tau y} = -J^y \tag{23}$$

$$\partial_\tau F^{\tau\eta} + \partial_x F^{x\eta} + \partial_y F^{y\eta} + \frac{1}{\tau} F^{\tau\eta} = -J^\eta \tag{24}$$

3 Equations with longitudinal acceleration in 1 + 1 dimensional

This section explores the one-dimensional generalized Bjorken flow ($v_z \neq \frac{z}{t}$) along the z direction with velocity $u^\mu = \gamma(1, 0, 0, v_z) = (\cosh Y, 0, 0, \sinh Y)$. The non-central collisions can create a strong magnetic field outside the reaction plane, dominated by a y component. The magnetic field induces the electric field in the reaction plane, which is dominated by a x component due to Faraday and Hall effects [40,41]. In fact, because of electromagnetic fields, there is a pressure gradient that causes the boost invariant Bjorken flow condition ($v_z = \frac{z}{t}$) to be explicitly broken. What we look for is the effects of the EM fields on the longitudinal acceleration and the expansion of the flow.

We assume that the electric field is oriented in the x direction and the magnetic field is perpendicular to the reaction plane, pointing along the y direction in an inviscid fluid with finite electrical conductivity:

$$b^\mu = (0, 0, b^y, 0), \qquad e^\mu = (0, e^x, 0, 0) \tag{25}$$

We also consider that the fluid has longitudinal flow only, and the transverse flow is neglected. We parameterize the fluid four-velocity as follow:

$$u^\mu = \gamma(1, 0, 0, v_z) = (\cosh Y, 0, 0, \sinh Y). \tag{26}$$

that Y is fluid rapidity($v_z = \tanh Y$). The four-velocity in Milne coordinates becomes:

$$u^\mu = \left(\cosh(Y - \eta), 0, 0, \frac{\sinh(Y - \eta)}{\tau}\right) = \bar{\gamma}\left(1, 0, 0, \frac{\tanh(Y - \eta)}{\tau}\right)$$

$$= \bar{\gamma}\left(1, 0, 0, \frac{\bar{v}}{\tau}\right) \tag{27}$$

where $\bar{\gamma} = \cosh(Y - \eta)$, and $\bar{v} = \tanh(Y - \eta)$. Thus, we obtain:

$$D = \bar{\gamma}\left(\partial_\tau + \frac{1}{\tau}\bar{v}\partial_\eta\right), \quad \Theta = \bar{\gamma}\left(\bar{v}\partial_\tau Y + \frac{1}{\tau}\partial_\eta Y\right) \tag{28}$$

Regarding the above setup, for conservation Eqs. (14)–(15) we can write:

$$(\tau\partial_\tau + \bar{v}\partial_\eta)\epsilon + (\epsilon + P)(\tau\bar{v}\partial_\tau Y + \partial_\eta Y) = \frac{1}{\bar{\gamma}}\tau\sigma e_x^2 \tag{29}$$

$$(\epsilon + P)\partial_\tau u^i + \partial^i P = 0 \tag{30}$$

$$(\epsilon + P)(\tau\partial_\tau + \bar{v}\partial_\eta)Y + (\tau\bar{v}\partial_\tau + \partial_\eta)P = \frac{\sigma\tau}{\bar{\gamma}}e_x b_y \tag{31}$$

Further, inserting the initial condition (25) and (27) into Maxwell's equations (17)–(24) give:

$$\partial_x e_x = \partial_y e_x = \partial_x b_y = \partial_y b_y = 0 \tag{32}$$

$$\partial_\tau\left[\tau(\bar{\gamma}b_y + \bar{\gamma}\bar{v}e_x)\right] + \partial_\eta\left[\bar{\gamma}\bar{v}b_y + \bar{\gamma}e_x\right] = 0 \tag{33}$$

$$\partial_\tau\left[\tau(\bar{\gamma}e_x + \bar{\gamma}\bar{v}b_y)\right] + \partial_\eta\left[(\bar{\gamma}\bar{v}e_x + \bar{\gamma}b_y)\right] = -\sigma\tau e_x \tag{34}$$

3.1 Perturbative solutions of RRMHD equations with acceleration

We now move on to explore perturbative solutions of the conservation equations in the presence of weak electric and magnetic fields on the longitudinal expansion of the flow. We suppose that the magnitude of electromagnetic fields is suppressed by the energy density of the fluid, $\frac{(b_y^2 + e_x^2)}{\epsilon} \ll 1$ which is not far from reality [31]. It is known that the typical magnetic field produced in Au–Au peripheral collisions at $\sqrt{s_{NN}} = 200$ GeV is estimated $|eB| \approx 5 \sim 10m_\pi^2$ at $\tau = 0$ after a RHIC collision. Assuming the magnitude of the initial energy density of the medium $\epsilon_c = T_0^4 \approx (300\,\text{MeV})^4$ at the initial proper time $\tau_0 = 0.6$ fm, and also assuming that the initial electromagnetic field is reduced to a smaller size by ten times at $\tau = 0.6$ fm, one finds $b_y^2/\epsilon_c \approx 0.17 \sim 0.68$ [31]. Here, we consider $m_\pi \approx 150$ MeV and $e^2 = 4\pi/137$. Consequently, the weak-field expansion could be a fair approximation for the electromagnetic fields generated in the relativistic heavy-ion collisions.

The electromagnetic fields are oriented in the transverse plane and are perpendicular to the longitudinal direction. We assume that the electromagnetic fields only depend on the proper time τ and rapidity η for a fluid following the longitudinal expansion with an acceleration. Since we investigate the propagation of small perturbations of EM field in a relativistic plasma, we consider these fields with a small expansion parameter (λ_1). Then, we perform small fluctuations around a homogeneous background and keep in the equations only linear sentences in the fluctuations consisting of up to $O(\lambda_1^2)$. In the end, the expansion parameter in calculations will be set to unity.

Therefore, we have the following setup in Milne coordinates:

$$b^\mu = (0, 0, \lambda_1 b_y, 0), \qquad e^\mu = (0, \lambda_1 e_x, 0, 0)$$

$$\epsilon(\tau, \eta) = \epsilon_0(\tau) + \lambda_1^2\epsilon_1(\tau, \eta), \qquad \epsilon_0(\tau) = \epsilon_c\left(\frac{\tau_0}{\tau}\right)^{1+\kappa} \tag{35}$$

Here τ_0 is an initial time, and ϵ_c represents the initial energy density of the medium at τ_0. Moreover, we assume:

$$Y(\tau, \eta) = \lambda(\tau, \eta)\eta = (1 + \lambda^*(\tau, \eta))\eta \longrightarrow Y - \eta = \lambda^*(\tau, \eta)\eta \tag{36}$$

where λ^* is a very small constant ($0 \leq \lambda^* \ll 1$) and $\lambda(\tau, \eta) = 1 + \lambda^*(\tau, \eta)$ is defined as acceleration parameter [37].

Besides, we consider $(Y - \eta) \ll 1$, so we have:

$$\bar{\gamma} = \cosh(Y - \eta) \simeq 1 \tag{37}$$

$$\bar{v} = \tanh (Y - \eta) \simeq (Y - \eta) = \lambda^* \eta = \lambda_1^2 v \tag{38}$$

Thus, the four-velocity in Milne coordinates becomes:

$$u^\mu = \left(\cosh (Y - \eta), 0, 0, \frac{\sinh(Y - \eta)}{\tau} \right) \simeq \left(1, 0, 0, \lambda_1^2 \frac{v}{\tau} \right) \tag{39}$$

Substituting this setup in conservation Eqs. (29)-(31) up to $O(\lambda_1^2)$, we will have:

$$\partial_\tau \epsilon_1 + \frac{(1 + \kappa)\epsilon_1}{\tau} + \frac{(1 + \kappa)\tau_0^{\kappa+1}\epsilon_c}{\tau^{\kappa+2}} \partial_\eta v = \sigma e_x^2 \tag{40}$$

$$(\epsilon + P)\partial_\tau u^i + \partial^i P = 0 \tag{41}$$

$$\partial_\eta \epsilon_1 + \frac{(1 + \kappa)\tau_0^{\kappa+1}\epsilon_c}{\kappa \tau^\kappa} \partial_\tau v - \frac{(\kappa^2 - 1)\tau_0^{\kappa+1}\epsilon_c}{\kappa \tau^{\kappa+1}} v = \frac{\sigma \tau}{\kappa} e_x b_y \tag{42}$$

where we regard the pressure to be proportional to the energy density as $P = \kappa \epsilon$ and κ is a constant. By considering a uniform pressure in the transverse plane, the second term in Eq. (41) will disappear; thus, we notice that if the velocities in the x and y directions are initially zero, they will remain zero at a later time. However, because of electromagnetic fields, there is a pressure gradient given in the η direction, so Eq. (42) explicitly breaks the Bjorken flow ($v_z = \frac{z}{t}$) condition, just as we supposed. In fact, there is an acceleration of the fluid by the EM fields.

What's more, applying the above initial condition, Maxwell's equations (33) and (34) up to $O(\lambda_1^2)$ are reduced to the following forms:

$$\partial_\tau b_y + \frac{1}{\tau}\partial_\eta e_x + \frac{b_y}{\tau} = 0 \tag{43}$$

$$\partial_\tau e_x + \frac{1}{\tau}\partial_\eta b_y + \frac{e_x}{\tau} + \sigma e_x = 0 \tag{44}$$

and the combination of two Eqs. (40) and (42) gives an in-homogeneous equation for $v(\tau, \eta)$:

$$(\kappa + 1)\tau_0^{\kappa+1}\epsilon_c \tau^{-\kappa-2}\left(\kappa \partial_\eta^2 v + \tau(\kappa - 2)\partial_\tau v - \tau^2 \partial_\tau^2 v \right)$$

$$+ \sigma e_x \left(\tau \partial_\tau b_y - 2\kappa \partial_\eta e_x \right) + \sigma b_y \left((\kappa + 2)e_x + \tau \partial_\tau e_x \right) = 0 \tag{45}$$

that directs us to the calculation of λ^* and the acceleration parameter. For this purpose, we first calculate the electromagnetic fields. Using Eqs. (43) and (44), we can obtain the following results:

$$-\partial_\eta^2 e_x + \tau^2 \partial_\tau^2 e_x + (3\tau + \sigma \tau^2)\partial_\tau e_x + (1 + 2\sigma \tau)e_x = 0 \tag{46}$$

$$-\partial_\eta^2 b_y + \tau^2 \partial_\tau^2 b_y + (3\tau + \sigma \tau^2)\partial_\tau b_y + (1 + \sigma \tau)b_y = 0 \tag{47}$$

In order to solve the above equations, we consider the electric and magnetic fields as:

$$e_x(\tau, \eta) = g(\eta)f(\tau)$$

$$b_y(\tau, \eta) = s(\eta)h(\tau) \tag{48}$$

If we substitute Eq. (48) into Eqs. (43) and (44), we have:

$$\tau h'(\tau) + h(\tau) = Cf(\tau) \tag{49}$$

$$g'(\eta) = -Cs(\eta) \tag{50}$$

and:

$$\tau f'(\tau) + (1 + \sigma\tau)f(\tau) = C'h(\tau) \tag{51}$$

$$s'(\eta) = -C'g(\eta) \tag{52}$$

Also, putting Eq. (48) in Eqs. (46) and (47) and utilising the method of the separation of variables, we can obtain:

$$\frac{d^2g(\eta)}{d\eta^2} = m^2 g(\eta) \tag{53}$$

$$\frac{d^2s(\eta)}{d\eta^2} = n^2 s(\eta) \tag{54}$$

By using the above relations, it is easy to demonstrate that $CC' = m^2 = n^2$ are separation constants, and for further application, we choose $m^2 = l(l+2) + 1$. Thus, the solutions of Eqs. (53) and (54) are given by:

$$g(\eta) = \sum_m e_m \cosh(m\eta) + e'_m \sinh(m\eta) \tag{55}$$

$$s(\eta) = \sum_m b_m \sinh(m\eta) + b'_m \cosh(m\eta) \tag{56}$$

It has been found out that the magnetic field generated by two nuclei passing each other in heavy-ion collisions should be an even function of η and most dominant at considerable rapidity after collisions [31]. The assumption is based on the external magnetic field led by moving nuclei after their collisions. Besides, according to Refs. [25,40,42], the electric field e_x has opposite directions at positive and negative rapidity. Also, at mid-rapidity ($\eta = 0$), the electric field is zero, but the magnetic field b_y has a nonzero value. Hence, it seems that the external electric field is an odd function of η, and the external magnetic field is an even function of η. To keep our calculation simple, we assume that the entire coupled electromagnetic fields have the same rapidity profile as the external ones. Based on the above discussion, in our setup, we expect the magnetic field to be an even function of η, and the electric field an odd function of η; thus:

$$s(\eta) = \sum_m b'_m \cosh(m\eta), \qquad g(\eta) = \sum_m e_m \sinh(m\eta) \tag{57}$$

Let us solve Eq. (46). The equation is given by:

$$\tau^2 \frac{d^2f(\tau)}{d\tau^2} + (3\tau + \sigma\tau^2)\frac{df(\tau)}{d\tau} + \left(-l(l+2) + 2\sigma\tau\right)f(\tau) = 0 \tag{58}$$

Then, we consider $f(\tau) = \tau^l G(\tau) = \tau^l \sum_{n=0}^{\infty} a_n \tau^n$ to be a power series function. When it is substituted into the above differential equation, we find $G(\tau)$ obeys by:

$$\frac{d^2G(\tau)}{d\tau^2} + \left(\sigma + \frac{2l+3}{\tau}\right)\frac{dG(\tau)}{d\tau} + \sigma\frac{(l+2)}{\tau}G(\tau) = 0 \tag{59}$$

and it's analytical solution is:

$$G(\tau) = C_{l1}e^{-\frac{1}{2}\sigma\tau}\tau^{-l-\frac{3}{2}}\left(\sigma\tau I_{-\frac{1}{2}+l}\left(-\frac{1}{2}\sigma\tau\right) + (\sigma\tau + 4l + 2)I_{l+\frac{1}{2}}\left(-\frac{1}{2}\sigma\tau\right)\right)$$

$$+C_{l2}e^{-\frac{1}{2}\sigma\tau}\tau^{-l-\frac{3}{2}}\left(-\sigma\tau K_{-\frac{1}{2}+l}\left(-\frac{1}{2}\sigma\tau\right) + (\sigma\tau + 4l + 2)K_{l+\frac{1}{2}}\left(-\frac{1}{2}\sigma\tau\right)\right)$$

(60)

where I_α and K_α are the modified Bessel functions. The constant coefficients C_{l1} and C_{l2} are determined by physical conditions.

We know that $f(\tau)$ should be a well-behaved function at infinity; therefore, we can demonstrate that l must be: $l = -2, -3, \ldots$. Besides, we have chosen $m^2 = l(l+2) + 1$, so for $l = -2, -3, ..m^2 = 1, 2, 3, ...$ This means that m is an integer (we consider m to be positive).

Equivalently, the solution of $f(\tau)$ for different values of l can be written as follows:

$$f_1(\tau) = \frac{G_1(\tau)}{\tau^2} = C_{11}\frac{1}{\tau^2} - C_{12}\frac{e^{-\sigma\tau}(\sigma\tau + 1)}{\tau^2}$$

$$f_2(\tau) = \frac{G_2(\tau)}{\tau^3} = C_{21}\frac{(3 - \sigma\tau)}{\tau^3} + C_{22}\frac{e^{-\sigma\tau}(\sigma^2\tau^2 + 4\sigma\tau + 6)}{\tau^3}$$

$$f_3(\tau) = \frac{G_3(\tau)}{\tau^4} = C_{31}\frac{(20 - 8\sigma\tau - 8\sigma^2\tau^2)}{\tau^4} - C_{32}\frac{e^{-\sigma\tau}(\sigma^3\tau^3 + 9\sigma^2\tau^2 + 36\sigma\tau + 60)}{\tau^4}, \cdots$$

(61)

Also, we know if $\sigma \to \infty$, then e_x should tend to zero. Therefore, we have to set $C_{i1} = 0$, $i = 1, 2, 3, \ldots$.

Finally, the most general solution obtained for the electric field is:

$$e_x(\tau, \eta) = \sum_{m=1}^{\infty} e_m f_m(\tau)\sinh(m\eta)$$

$$= e_1\sinh(\eta)\frac{e^{-\sigma\tau}(1 + \sigma\tau)}{\tau^2} + e_2\sinh(2\eta)\frac{e^{-\sigma\tau}(6 + 4\sigma\tau + \sigma^2\tau^2)}{\tau^3}$$

$$+ e_3\sinh(3\eta)\frac{e^{-\sigma\tau}(60 + 36\sigma\tau + 9\sigma^2\tau^2 + \sigma^3\tau^3)}{\tau^4} + \cdots$$

(62)

where e_m are constants and should be determined. To find the time dependence of the magnetic field, we can replace the $e_x(\tau, \eta)$ from the above equation into Eq. (44). Then, the magnetic field is given by:

$$b_y(\tau, \eta) = F_1(\tau) + e_1\cosh(\eta)\frac{e^{-\sigma\tau}}{\tau^2} + e_2\cosh(2\eta)\frac{e^{-\sigma\tau}(6 + 2\sigma\tau)}{\tau^3}$$

$$+ e_3\cosh(3\eta)\frac{e^{-\sigma\tau}(60 + 24\sigma\tau + 3\sigma^2\tau^2)}{\tau^4} + \cdots$$

(63)

We also know that if $\sigma \to \infty$ then b_y tends toward $\frac{1}{\tau}$ [29]. Therefore, we have $F_1(\tau) = b_0\frac{\tau_0}{\tau}$. On the other hand, it is expected that the magnetic field will decay in vacuum ($\sigma \to 0$) as [6,32]:

$$b_y(\tau, 0) \approx b_1\frac{\tau_0^3}{\tau^3}$$

(64)

By using this relation, one can deduce that all coefficients of e_i should be zero except e_2. Consequently, the electric and magnetic fields can be written as:

$$e_x(\tau, \eta) = b_1 \frac{\tau_0^3}{\tau^3} e^{-\sigma\tau} \sinh(2\eta)(6 + 4\sigma\tau + \sigma^2\tau^2)$$

$$b_y(\tau, \eta) = b_0 \frac{\tau_0}{\tau}(1 - e^{-\sigma\tau}) + b_1 \frac{\tau_0^3}{\tau^3} e^{-\sigma\tau} \cosh(2\eta)(6 + 2\sigma\tau) \tag{65}$$

In order to evaluate our results, we consider the ideal RMHD, i.e. electrical conductivity is infinite ($\sigma \to \infty$). In this case, we have:

$$b_y(\tau) = b_0 \left(\frac{\tau_0}{\tau}\right), \quad e_x = 0 \tag{66}$$

which is consistent with previous studies.

To determine the acceleration parameter, we should look into Eq. (45), which consists of homogeneous and inhomogeneous solutions. When $e_x = 0$, we reach a homogeneous partial differential equation that is the result of the generalized Bjorken flow. According to the Ref. [42], and simplifying our calculation, we assume that λ^* only depends on the proper time τ in the absence of electromagnetic fields in hydrodynamic equations:

$$v^h(\tau, \eta) = \lambda^*(\tau)\eta \tag{67}$$

Thus, $\partial_\eta^2 v^h(\tau, \eta) = 0$ in Eq. (45), and the regular solution takes the form:

$$v^h(\tau, \eta) = A_0 \left(\frac{\tau_0}{\tau}\right)^{2/3} \eta \tag{68}$$

where $\kappa = \frac{1}{3}$ is chosen.

In order to obtain an inhomogeneous solution of Eq. (45), we substitute EM fields Eq. (65) and solve this differential equation. So, $v^{ih}(\tau, \eta)$ is:

$$v^{ih}(\tau, \eta) = \sigma\tau_0 \left(\frac{\tau_0}{\tau}\right)^{11/3} e^{-2\sigma\tau} \sinh(2\eta) \cosh(2\eta) H(x), \tag{69}$$

here $x = \sigma\tau$, and $H(x)$ satisfies the following equation:

$$2\epsilon_c \left(-x^2 H''(x) + \left(4x^2 + \frac{17}{3}x\right) H'(x) - \left(4x^2 + \frac{34}{3}x + \frac{17}{3}\right) H(x)\right)$$
$$= b_1^2 \left(8x^4 + 60x^3 + 199x^2 + 348x + 270\right) \tag{70}$$

Because of the electromagnetic fields, we are forced to consider λ dependent on proper time τ and rapidity η. Then, the acceleration parameter is given by:

$$\lambda(\tau, \eta) = 1 + A_0 \left(\frac{\tau_0}{\tau}\right)^{2/3} + \frac{\sigma\tau_0 \left(\frac{\tau_0}{\tau}\right)^{11/3} e^{-2\sigma\tau} \sinh(2\eta) \cosh(2\eta) H(x)}{\eta} \tag{71}$$

In the above equation, there are three terms. If the Bjorken model is considered with $e_x = 0$, it leads to $\lambda = 1$. However, if the Bjorken Model is generalized ($v_z \neq \frac{z}{t}$) with $e_x = 0$, then $\lambda = 1 + A_0 \left(\frac{\tau_0}{\tau}\right)^{2/3}$. Finally, the third term only exists if the plasma has the finite electrical conductivity($e_x \neq 0$).

Moreover, we can achieve the modification of energy density ϵ_1 from Eq. (42). We will explain the behavior of these physical quantities in the next section.

4 Results and discussions

In this section, our work is to provide a clear insight from the dynamical evolution and features of EM fields, which are given by Eq. (65). In addition, we will present the longitudinal evolution of the fluid, which manifests itself in the form of an acceleration parameter that is the effect of the generalized Bjorken model and of considering a finite electrical conductivity in the fluid. The acceleration parameter and the correction of energy density are obtained from our perturbation approach. These two quantities will help us understand the space-time evolution of the quark-gluon plasma in heavy-ion collisions.

In order to evaluate the EM fields from Eq. (65), and to fix the constants b_0, b_1, we consider the initial condition for the magnetic field at the mid-rapidity to be as $b(\tau_0, 0) = 0.0018 \frac{\text{GeV}^2}{\text{e}}$ [41]. Furthermore, we need to assume a simple relation between these two coefficients for the simplicity of our calculation. In fact, we will define $|\frac{b_1}{b_0}| = \alpha$ throughout this paper, and we will discuss the effects of different values of α on the evolution of QGP. First of all, at the mid-rapidity for each α and with applying the value of the initial magnetic field as $b(\tau_0, 0) = 0.0018 \frac{\text{GeV}^2}{\text{e}}$, we can obtain two parameters b_0 and b_1. Since the ratio of these two parameters (b_0 and b_1) is essential, we consider α in different orders. Due to the electric field being directed along the negative (positive) direction at positive (negative) rapidity [40], we choose b_1 with a negative sign. This choice also leads us to select b_0 with a negative sign; thus, the magnetic field points along the $-y$ direction.

At first, we investigated the dynamical evolution of EM fields. In Fig. 1, for different values of α, we have plotted the evolution of $b_y(\tau, \eta)$ as a function of τ at $\eta = 0$. These plots display that the presence of conducting medium delays the decay of the magnetic field; however, the α parameter, which comes from initial conditions, has a significant effect on the delay process of $b_y(\tau, \eta)$. Figure 1a reports the evolution of the magnetic field for $\alpha = 0.01$, and we can see that our result for $\sigma = 0.023$ fm^{-1} support previous results in [25]. For larger values of α (Fig. 1c, d) the decay behavior of the magnetic field is not sensitive to the variation of σ; thus, we select the order of α as $0.01 \sim 0.1$ whose effect of electrical conductivity is remarkable, and we can focus on the dependence of physical quantities to electrical conductivity.

We present a profile of $b_y(\tau, \eta)$ with respect to rapidity for different values of proper times and two values of σ, which is illustrated in Fig. 2a, b. Here, each curve refers to different values of proper time from $\tau = 0.5$ fm to $\tau = 3.5$ fm. As can be seen, the magnetic field increases with rapidity at fix time, and it tends to decrease with increasing time. Furthermore, the magnetic field tends to remain constant with the passage of time at a significant limit of η. The higher the electrical conductivity, the range of rapidity in which the magnetic field is stable becomes more extensive, and the amount of magnetic field is more valuable as well. A comparison between the curves in these figures reveals that the magnetic field increases around the small rapidities with rising the σ, whereas it decreases in large rapidities.

In Fig. 3, the time evolution of the electric field is shown at $\eta = -1$ with different values of the electric conductivity for $\alpha = 0.01$ (Fig. 3a), and $\alpha = 0.1$ (Fig. 3b). Similar to the magnetic field, the electric field decreases with increasing time, and it drops rapidly for the high value of σ. It also exhibits that the electric field has decreased into a faster decay process for a smaller value of α (Fig. 3a). We emphasize once more that the different values of α influence determining the constants of magnetic fields (b_0 and b_1) according to the initial conditions.

Figure 4a, b are the demonstration of $e_x(\tau, \eta)$ with respect to rapidity η for different values of the proper time (from $\tau = 0.5$ fm up to $\tau = 3.5$ fm) by considering two different values
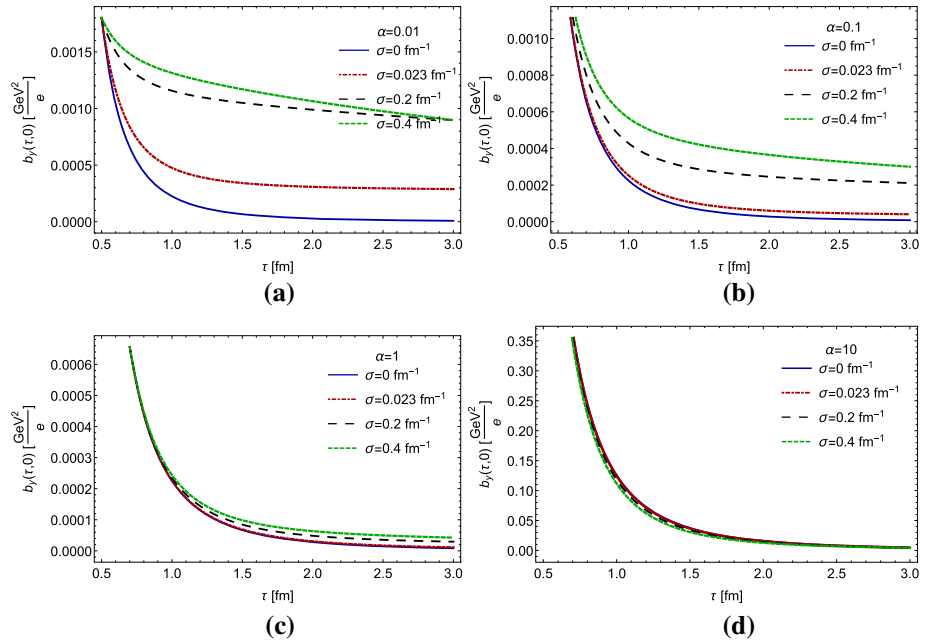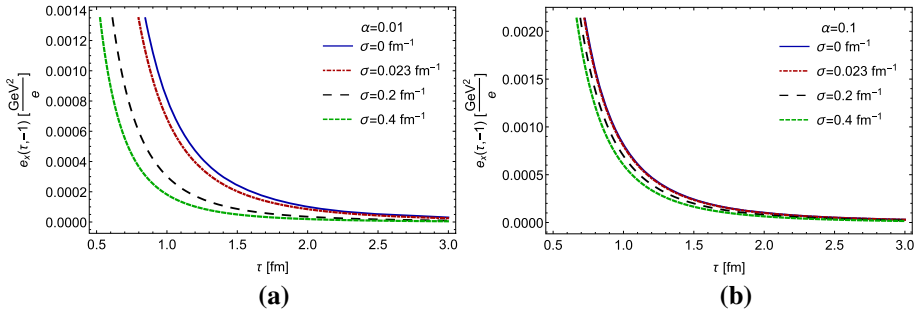
Fig. 1 The evolution of the magnetic field in terms of τ is plotted for different values of α at $\eta = 0$ with $\sigma = 0$ (blue solid curve), $\sigma = 0.023$ fm^{-1} (red dot-dashed curve), $\sigma = 0.2$ fm^{-1} (black dashed curve), and $\sigma = 0.4$ fm^{-1} (green dashed curve). As expected, increasing the electrical conductivity delays the decay of the magnetic field, which is more notable for $\alpha = 0.01$ (**a**), and $\alpha = 0.1$ (**b**)
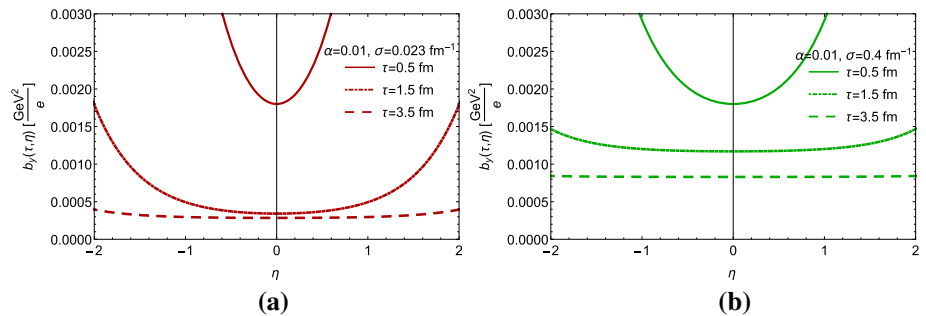

Fig. 2 The magnetic field in terms of η at **a** $\sigma = 0.023$ fm^{-1}, and **b** $\sigma = 0.4$ fm^{-1} is plotted for $\alpha = 0.01$. In two panels, the solid curves correspond to $\tau = 0.5$ fm, the dot-dashed curves to $\tau = 1.5$ fm, and the dashed curves to $\tau = 3.5$ fm. The magnetic field remains constant with the passage of time at a significant limit, and this range is more inclusive for higher electrical conductivity with the stronger amount of magnetic field (**b**)

of σ. It can be seen that the electric field is an odd function of η, and in central rapidity, the electric field is zero. Even though the electric field is stronger at large rapidities, this amount for $\sigma = 0.4$ fm^{-1} (Fig. 4a) is smaller than when $\sigma = 0.023$ fm^{-1} (Fig. 4b); thus, the high conductivity affects the electric field in fluid, and it will disappear quickly.

It is interesting to explore the acceleration parameter, which is obtained from Eq. (71). It consists of two critical parts: the effect of the generalized Bjorken model (GBM), which illustrates that the acceleration parameter is only dependent on the proper time τ, and the influence

Fig. 3 The time evolution of $e_x(\tau, \eta)$ is plotted for two different values of α at $\eta = -1$ with $\sigma = 0$ (blue solid curve), $\sigma = 0.023$ fm^{-1} (red dot-dashed curve), $\sigma = 0.2$ fm^{-1} (black dashed curve), and $\sigma = 0.4$ fm^{-1} (green dashed curve). As can be seen, the electric field decreases with increasing the electrical conductivity in a quicker process, which is more notable for $\alpha = 0.01$ at **(a)**
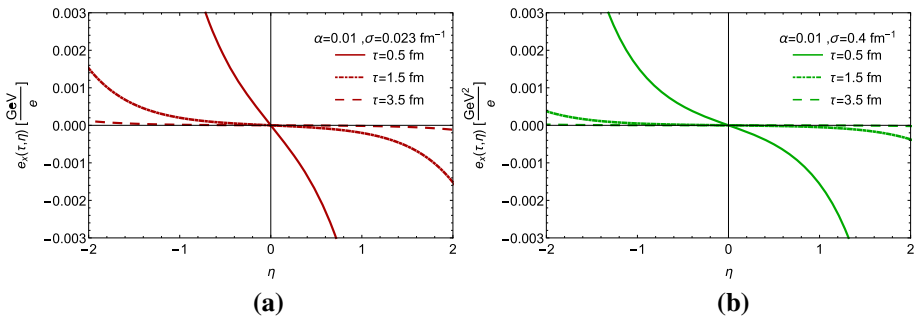

Fig. 4 The electric field in terms of η is outlined at **a** $\sigma = 0.023$ fm^{-1}, and **b** $\sigma = 0.4$ fm^{-1}. The value of $\alpha = 0.01$ is chosen. In these plots, the solid curves are related to $\tau = 0.5$ fm, the dot-dashed curves to $\tau = 1.5$ fm, and the dashed curves to $\tau = 3.5$ fm. The electric field is stronger at large rapidities, but the high conductivity causes the electric field to decay quickly in earlier times

of the existence of EM fields in the fluid, which shows that the acceleration parameter should be considered as a function of τ and η.

Figure 5 is an illustration of evolution of $\lambda(\tau, \eta)$ in terms of τ for different values of rapidity. We choose the electrical conductivity as $\sigma = 0.023$ fm^{-1}, and $\alpha = 0.01$. The EM fields with finite electrical conductivity create a considerable acceleration with a negative sign, especially at the early times, which is more significant at large rapidities and fades the effect of the generalized Bjorken model. However, in late time the effect of the EM fields on the acceleration parameter becomes slight, and the acceleration parameter tends to a fixed amount of more than 1. Furthermore, the dependence of the acceleration parameter to η for fixed τ is displayed in Fig. 6. It can be seen that the acceleration parameter decreases when the absolute amount of η increases; however, for the late time, we have a plateau. According to this plot, increasing η decreases the acceleration parameter, and with the passage of time, the reducing process of $\lambda(\tau, \eta)$ is happening in an extended range of rapidity.

In order to discuss the dependence of the acceleration parameter on the matter, we investigate the effects of electric conductivity on the λ because one of the most important proprieties of the QGP is its electric conductivity. We know that at the mid-rapidity, the electric field is zero; therefore, we are not able to investigate the effect of σ on the accelerated fluid. Thus, we consider the effect of electrical conductivity σ on acceleration parameter $\lambda(\tau, \eta)$ at $\eta = 1$.
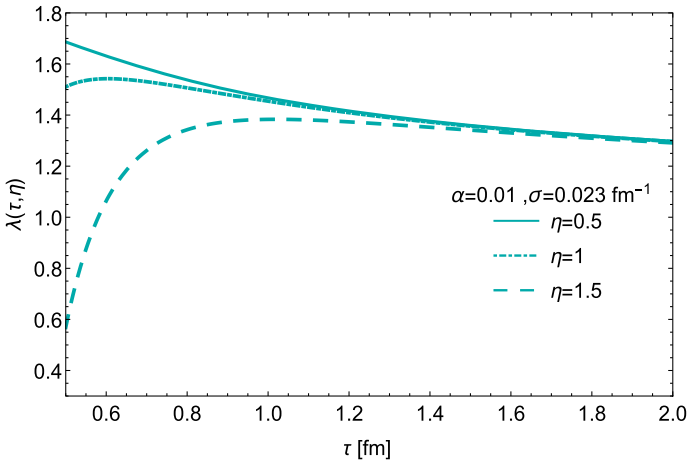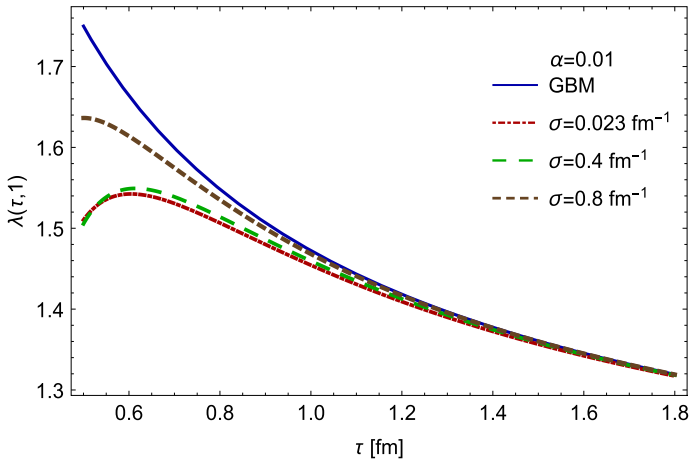
Fig. 5 Acceleration parameter $\lambda(\tau, \eta)$ in terms of proper time τ is plotted for $\sigma = 0.023\,\text{fm}^{-1}$ and $\alpha = 0.01$. The solid curve, dot-dashed curve, and the dashed curve corresponds to $\eta = 0.5, 1, 1.5$, respectively. As expected, the acceleration parameter tends to a fixed amount of more than 1
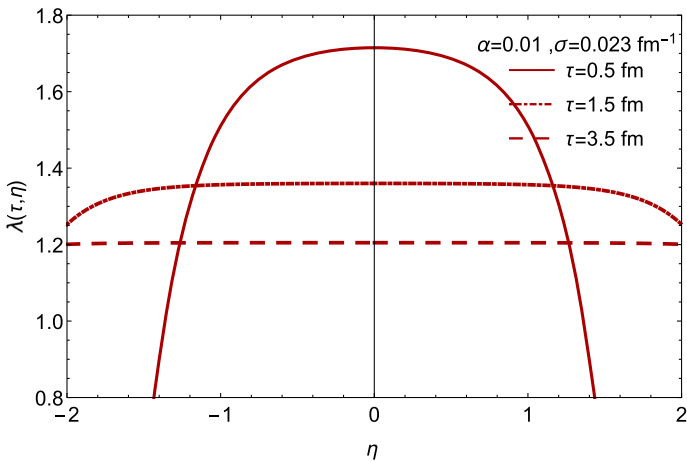
Fig. 6 Acceleration parameter $\lambda(\tau, \eta)$ in terms of η is illustrated for $\sigma = 0.023\,\text{fm}^{-1}$, and $\alpha = 0.01$ with $\tau = 0.5, 1.5, 3.5\,\text{fm}$ (solid, dot-dashed, and dashed curves, respectively). As it turns out, increasing the η decreases the acceleration parameter. Furthermore, at the late time, the reducing process of $\lambda(\tau, \eta)$ is occurring on a broader range of rapidities

In Fig. 7, the effect of electrical conductivity on acceleration parameter is examined. Since the electric field is expected to decay much faster in high conductivity (Fig. 3), the effect of EM fields on the acceleration of fluid is negligible, and $\lambda(\tau, \eta)$ tends to be similar to the generalized Bjorken model ($v_z \neq \frac{z}{t}$). The remarkable point in our results is that the acceleration parameter can also be found in fluid with high conductivity (or ideal fluid; $\sigma \to \infty$).

In the end, a discussion on the effects of the EM fields on energy density is in order. We can obtain the correction of energy density by Eq. (42). We remind the reader of the fact that the total energy density is $\epsilon = \epsilon_0(\tau) + \epsilon_1(\tau, \eta)$ and that the latter is the component that is truly affected by the acceleration of the fluid. Now, if we consider the homogeneous solution

Fig. 7 The acceleration parameter $\lambda(\tau, \eta)$ in terms of τ is indicated for $\eta = 1$ and $\alpha = 0.01$. In this plane, the blue solid curve corresponds to the generalized Bjorken model (GBM), the red dot-dashed curve to $\sigma = 0.023$ fm^{-1}, the green dashed curve to $\sigma = 0.4$ fm^{-1}, and the brown dashed curve to $\sigma = 0.8$ fm^{-1}. As shown, the σ influences the acceleration parameter, and in high conductivity, it leads to the generalized Bjorken model

of Eq. (45) as v^h (Eq. (68)), which is the result of the generalized Bjorken flow, the correction of energy density will disappear. Thus, the energy density is the same as the Bjorken model $\epsilon_0(\tau) = \epsilon_c (\frac{\tau_0}{\tau})^{1+\kappa}$. Therefore, the correction of energy density is entirely affected by EM fields and electrical conductivity.

The ratio of energy density $\epsilon(\tau, \eta)/\epsilon_0$ in terms of proper time τ is exhibited in Fig. 8 for $\sigma = 0.023$fm^{-1}, and different values of rapidities. As is evident, the energy density profile is very similar to the acceleration parameter (Fig. 5). In this plot, we have made a comparison between the accelerated fluid and the Bjorken model. We notice that for $\eta = 0$, the effect of the EM fields on the energy density could be ignored. However, the energy density rate decays faster than the Bjorken model at the $\eta \neq 0$ and early time. Also, in Fig. 9, we demonstrate $\epsilon(\tau, \eta)/\epsilon_0$ in terms of rapidity for fixed proper times. It can be seen that at the early times, the plot has a Gaussian distribution, while at the late time, it becomes a plateau around the small rapidities.

To emphasize the effect of the electrical conductivity on the energy density, we have plotted the time evolution of $\epsilon(\tau, \eta)/\epsilon_0$ at the mid-rapidity by considering several values of σ. As shown in Fig. 10, the reduction of energy density is modified most significantly in the early times. Due to the rapid decay of the electric field in high conductivity, the influence of σ on the perturbation of energy density will disappear, and the ratio of energy density tends toward the Bjorken model. In addition, $\epsilon(\tau_0, \eta)/\epsilon_0$ in terms of η at the fixed proper time $\tau_0 = 0.5$ fm is illustrated in Fig. 11. According to this figure, by increasing the value of the electrical conductivity σ, the energy density profile is directed to a plateau because in high conductivity, the energy density is not sensitive to the rapidity and its behavior leads to the Bjorken model.
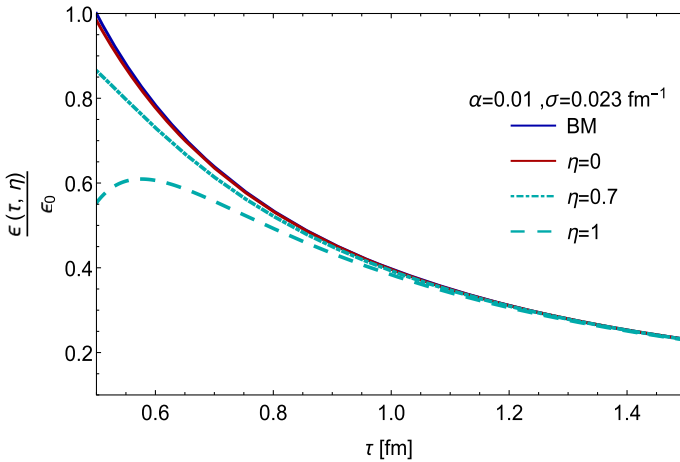
Fig. 8 The ratio of energy density $\epsilon(\tau, \eta)/\epsilon_0$ in terms of τ is outlined for $\sigma = 0.023$ fm^{-1}, and $\alpha = 0.01$. It is plotted for different rapidities and in comparison with the Bjorken model. The blue solid curve is related to the Bjorken model (BM), the red solid curve to $\eta = 0$, the dot-dashed curve to $\eta = 0.7$, and the dashed curve to $\eta = 1$
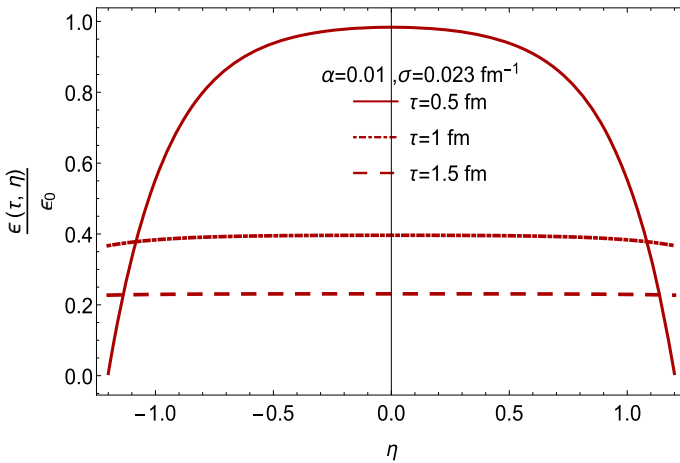

Fig. 9 The $\epsilon(\tau, \eta)/\epsilon_0$ in terms of rapidity η is plotted for $\sigma = 0.023$ fm^{-1}, and $\alpha = 0.01$ with $\tau = 0.5, 1.5, 3.5$ fm (solid, dot-dashed, and dashed curves, respectively). At the late time, the Gaussian form of energy density transforms to a plateau around the small rapidities

4.1 The transverse velocity and transverse momentum spectrum in the presence of electromagnetic fields

In the previous sections, we have obtained analytical solutions for the EM fields and energy density. Now we can apply these results to estimate the transverse momentum spectrum emerging from the magneto-hydrodynamic solutions. However, in our calculations developed in the previous sections, the transverse dynamics has been discarded. Here, we compute the transverse flow only as an effect due to the currents generated by the electric field and not like a flow coming from gradient pressure. Our goal is to predict the influence of the electric field
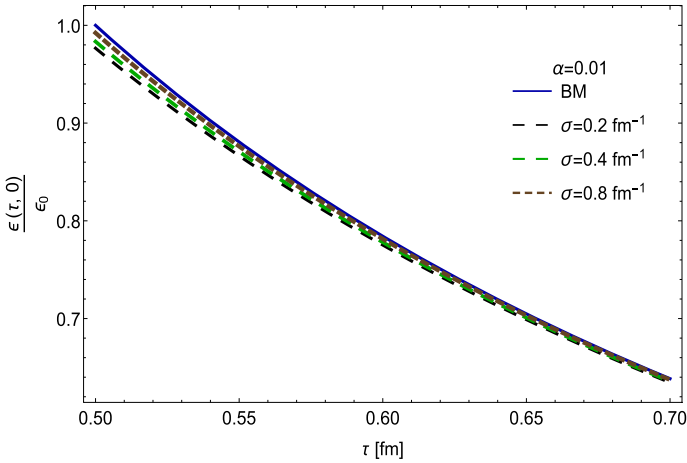
Fig. 10 The time evolution of the $\epsilon(\tau, \eta)/\epsilon_0$ is plotted for $\alpha = 0.01$, and $\eta = 0$. The blue solid curve, the black dashed curve, the green dashed curve, and the brown dashed curve corresponds to the Bjorken model, $\sigma = 0.2$ fm^{-1}, $\sigma = 0.4$ fm^{-1}, and $\sigma = 0.8$ fm^{-1}, respectively. As can be seen, increasing the electrical conductivity causes the decrease of the energy density to become negligible and led to the Bjorken model
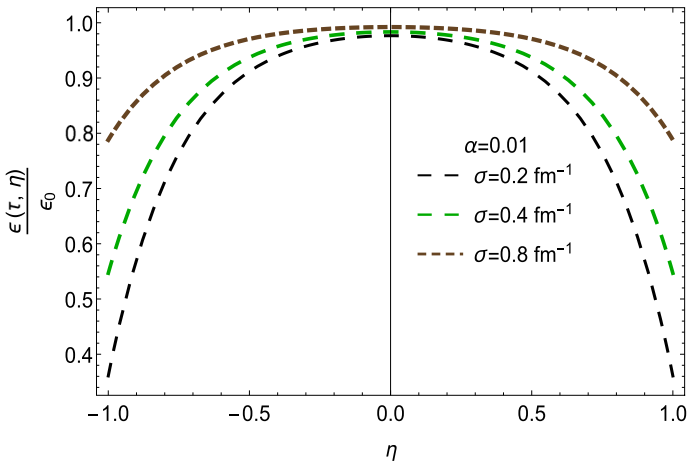
Fig. 11 The ratio of energy density $\epsilon(\tau, \eta)/\epsilon_0$ in terms of η is plotted for $\alpha = 0.01$ at early proper time $\tau = 0.5$ fm. The black, green, and brown dashed curves correspond to $\sigma = 0.2, 0.4, 0.8$ fm^{-1}, respectively. The profile of $\epsilon(\tau, \eta)/\epsilon_0$ tends to a plateau in high conductivity

in the final state of the Pion and Proton transverse spectrum. We assume that the transverse flow v_x, which results from the presence of the electromagnetic field, is much smaller than the velocity of the expanding plasma ($v_x << 1$). We also discard the transverse hydrodynamic expansion, which is induced by gradient pressure.

To examine the effects of electromagnetic fields on the transverse momentum spectrum, we need to obtain the velocity of charged particles such as proton and pion in the spectrum. From $e^\mu = (0, e^x, 0, 0)$ and the electrical conductivity σ, it would be straightforward to take the electric current density as Eq. (7): $J^\mu = \sigma e^\mu$. However, for our purposes, what we need is the transverse velocity, which is created by the current density. Besides, we know

that when an electric field is established in a conductivity fluid, the charge carriers (assumed positive) acquire a drift speed in the direction of the electric field, and this velocity is related to the current density by: $J^\mu = nqv^\mu$, where n is the particle density. We look for stationary currents in the local fluid rest frame for the u and d quarks and antiquarks. Thus, with setting $q = +2e/3$ for u and $q = +e/3$ for $\bar{d}$, the charge density which is created by the positively charged species obtains as:

$$J^\mu = \frac{2}{3} n_u \, e \, v_u^\mu + \frac{1}{3} n_{\bar{d}} \, e \, v_{\bar{d}}^\mu \tag{72}$$

For the sake of simplicity, we assume that the particle density for this quark and antiquark is the same and that these particles have a similar share in the transverse velocity of the fluid. With these assumptions, the transverse velocity becomes:

$$v_x = \frac{\sigma e_x}{ne} \tag{73}$$

where e_x can be taken from Eq. (65).

Now, we can obtain an analytical solution of the transverse velocity in the presence of a weak electromagnetic field and utilise these results to estimate the transverse momentum spectrum emerging from the magneto-hydrodynamic solutions. Here, the fluid four-velocity, which approximately describes the boost invariant longitudinal expansion and the transverse expansion, is given by:

$$u^\mu = (u^\tau, u_{x_\perp}, 0, u^\eta) \tag{74}$$

In this section we assume $u^\eta \simeq 0$. We ignore the impact of the electromagnetic fields on the acceleration of the longitudinal expansion of the fluid. As such, the only nonzero components of u^μ are u^τ which describes the boost-invariant longitudinal expansion, and $u_{x_\perp}$, which describes the transverse expansion.

From the local equilibrium hadron distribution, the transverse spectrum is calculated at the freeze-out surface via the Cooper–Frye (CF) formula:

$$S = E \frac{d^3 N}{dp^3} = \frac{dN}{p_T dp_T dy d\varphi} = \int d\Sigma_\mu p^\mu \exp\left(\frac{-p^\mu u_\mu}{T_f}\right) \tag{75}$$

We notice that T_f is the temperature at the freeze-out surface. It is the isothermal surface in space-time at which the temperature of the inviscid fluid is related to the energy density as $T \propto \epsilon^{1/4}$. It must satisfy $T(\tau, \eta) = T_f$.

In our calculations:

$$d\Sigma_\mu = (-1, 0, 0, 0)\tau_f x_\perp dx_\perp d\varphi d\eta \tag{76}$$

$$p^\mu = (m_T \cosh(Y - \eta), p_T \cos(\varphi_p - \varphi), r \, p_T \cos(\varphi_p - \varphi), \tau_f m_T \sinh(Y - \eta)) \tag{77}$$

We mention that $x_\perp$ is the transverse (cylindrical) radius, $\eta = \frac{1}{2} \log \frac{t+z}{t-z}$ the longitudinal rapidity (hyperbolic arc angle), and the azimuthal angle φ_p belonging to the spacetime point x^μ. Also, p_T is the detected transverse momentum, $m_T = \sqrt{m^2 + p_T^2}$ the corresponding transverse mass, while Y is the observed longitudinal rapidity.

The final transverse spectrum is calculated at the freeze-out surface via the Cooper–Frye(CF) formula is given by [25,42]:

$$S = \frac{g_i}{2\pi} \int_0^{x_f} m_T x_\perp \tau_f(\eta) K_1 \left(\frac{m_T u_\tau}{T_f}\right) I_0 \left(\frac{m_T u_{x_\perp}}{T_f}\right) dx_\perp \tag{78}$$
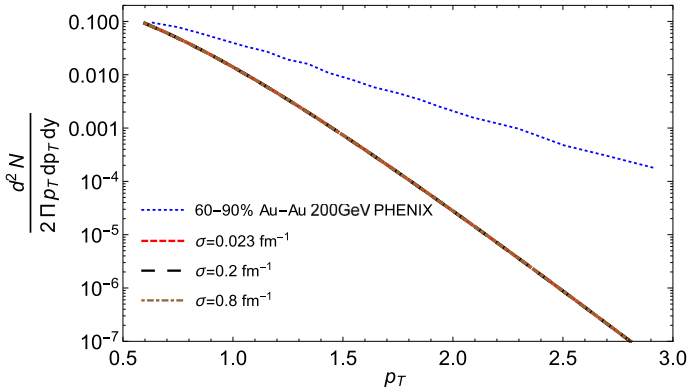
Fig. 12 The Proton transverse spectrum from non-central Au–Au collisions. The red, black, and brown curves correspond to $\sigma = 0.023, 0.2, 0.8$ fm^{-1}, respectively, and the blue curve corresponds to PHENIX data
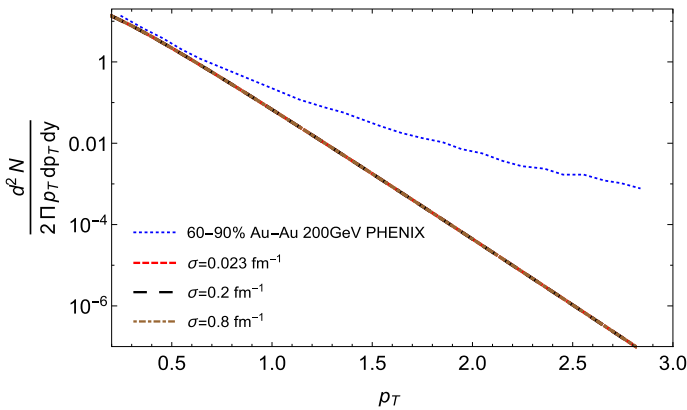
Fig. 13 The Pion transverse spectrum from non-central Au–Au collisions. The red, black, and brown curves correspond to $\sigma = 0.023, 0.2, 0.8$ fm^{-1}, respectively, and the blue curve corresponds to PHENIX data

where $u_\tau = 1$, $u_{x_\perp} = \gamma v_x = v_x$, and $\tau_f(\eta)$ is the solution of the $T(\tau_f, \eta) = T_f$, where T_f is the temperature at the freeze-out surface. For the energy density, the relation $\epsilon = \epsilon_0(\tau) + \epsilon_1(\tau, \eta)$ is applied where $\epsilon_1(\tau, \eta)$ is the correction of energy density and is obtained from Eq. (42). Moreover, $g_i = 2$ is degeneracy factor for the Proton or Pion.

The transverse spectrum Eq. (78) is illustrated in Figs. 12 and 13 for three different values of electrical conductivity for rapidity $\eta = 1$ and $\alpha = 0.01$, and they are compared with experimental results obtained at PHENIX [43] in non-central Au–Au collisions. Here, we consider $T_f = 130$ MeV. Our spectra appear to underestimate the experimental data, but their behavior with p_T has the correct trend of decreasing monotonically. Although the conductivity significantly affects the electric field, magnetic field and energy density, the final spectrum is not sensitive to the σ parameter.

5 Conclusion and outlook

The magnitudes and the evolution of electromagnetic fields play a crucial role in estimating possible observable effects of the de-confinement and chiral phase transitions in heavy-ion collisions. There are many studies that have investigated electromagnetic field strength and its evolution. It has been known in the initial stage that the magnitude of the magnetic field falls rapidly with time ($|B_y| \sim \frac{1}{\tau^3}$); however, the presence of the hot QGP may increase the lifetime of the strong magnetic field.

In the present study, we have examined the $1 + 1$ longitudinal acceleration expansion motion of a resistive fluid with the electrical conductivity σ in the RRMHD framework in the presence of EM fields. We have considered that the QGP medium is created a short time after collisions with the generalized Bjorken longitudinal ($v_z \neq \frac{z}{t}$) along the z direction, the magnetic field pointed in y, and the electric field pointed in x directions. We have investigated the propagation of small perturbations of the EM field and its effect on the correction of energy density and the acceleration parameter. Since we are interested in the longitudinal expansion, all quantities depended on proper time τ and space-time rapidity η. By applying the initial conditions in Maxwell's equations, we have computed analytical solutions for the electric and magnetic fields in the conducting fluid with the electrical conductivity σ, and the energy and Euler equations have provided us with an accurate description of the acceleration parameter of fluid and the perturbation of the energy density.

We have demonstrated the time evolution of the magnetic and electric fields to the τ and η variables and as well as the effect of the σ parameter in the evolution. The analytical results that we have obtained are in satisfactory agreement with the previous ones, in which the ideal RMHD is considered, and the electrical conductivity is infinite. Furthermore, we have found a picture of the evolution of the acceleration of fluid and energy density. Our analytic solutions are worth acquiring deeper understandings for more realistic numerical results.

References

1. P. Romatschke, U. Romatschke, Viscosity information from relativistic nuclear collisions: How perfect is the fluid observed at RHIC? Phys. Rev. Lett. **99**, 172301 (2007)
2. D.E. Kharzeev, L.D. McLerran, H.J. Warringa, The effects of topological charge change in heavy ion collisions: event by event P and CP violation. Nucl. Phys. A **803**, 227 (2008)
3. V. Skokov, A. Illarionov, V. Toneev, Estimate of the magnetic field strength in heavy-ion collisions. Int. J. Mod. Phys. A **24**, 5925 (2009)
4. Y. Zhong, C. Yang, X. Cai, S. Feng, A systematic study of magnetic field in relativistic heavy-ion collisions in the RHIC and LHC energy regions. Adv. High Energy Phys. **2014**, 193039 (2014)
5. L. McLerran, V. Skokov, Comments about the electromagnetic field in heavy-ion collisions. Nucl. Phys. A **929**, 184 (2014)
6. B.G. Zakharov, Electromagnetic response of quark-gluon plasma in heavy-ion collisions. Phys. Lett. B **737**, 262 (2014)
7. S.A. Voloshin, Parity violation in hot QCD: how to detect it. Phys. Rev. C **70**, 057901 (2004)
8. K. Fukushima, D.E. Kharzeev, H.J. Warringa, The chiral magnetic effect. Phys. Rev. D **78**, 074033 (2008)
9. B.I. Abelev et al., [STAR Collaboration], Observation of charge-dependent azimuthal correlations and possible local strong parity violation in heavy ion collisions. Phys. Rev. C **81**, 054908 (2010)
10. D.E. Kharzeev, H. Yee, Chiral magnetic wave. Phys. Rev. D **83**, 085007 (2011)
11. Y. Burnier, D.E. Kharzeev, J. Liao, H. Yee, Chiral magnetic wave at finite baryon density and the electric quadrupole moment of quark-gluon plasma in heavy ion collisions. Phys. Rev. Lett. **107**, 052303 (2011)
12. J. Bloczynski, X.G. Huang, X. Zhang, J. Liao, Azimuthally fluctuating magnetic field and its impacts on observables in heavy-ion collisions. Phys. Lett. B **718**, 1529 (2013)
13. K. Tuchin, Electromagnetic field and the chiral magnetic effect in the quark gluon plasma. Phys. Rev. C **91**, 064902 (2015)

14. W.T. Deng, X.G. Huang, Electric fields and chiral magnetic effect in Cu + Au collisions. Phys. Lett. B **742**, 296 (2015)

15. J. Adam et al., [ALICE Collaboration],Charge-dependent flow and the search for the chiral magnetic wave in Pb–Pb collisions at $\sqrt{s_{NN}} = 2.76$ TeV, Phys. Rev. C **93**(4), 044903 (2016)

16. Q. Li et al., Observation of the chiral magnetic effect in $ZrTe_5$. Nat. Phys. **12**, 550 (2016)

17. D.E. Kharzeev, J. Liao, S.A. Voloshin, G. Wang, Chiral magnetic and vortical effects in high-energy nuclear collisions—a status report. Prog. Part. Nucl. Phys. **88**, 1 (2016)

18. J. Xiong et al., Signature of the chiral anomaly in a Dirac semimetal: a current plume steered by a magnetic field, arXiv:1503.08179 [cond-mat.str-el]

19. W.T. Deng, X.G. Huang, Event-by-event generation of electromagnetic fields in heavy-ion collisions. Phys. Rev. C **85**, 044907 (2012)

20. K. Tuchin, Time and space dependence of the electromagnetic field in relativistic heavy-ion collisions. Phys. Rev. C **88**, 024911 (2013)

21. K. Tuchin, Particle production in strong electromagnetic fields in relativistic heavy-ion collisions. Adv. High Energy Phys. **2013**, 490495 (2013)

22. K. Tuchin, Electromagnetic fields in high energy heavy-ion collisions. Int. J. Mod. Phys. E **23**(1), 1430001 (2014)

23. A. Bzdak, V. Skokov, Event-by-event fluctuations of magnetic and electric fields in heavy ion collisions. Phys. Lett. B **710**, 171 (2012)

24. G.S. Balia et al., Effects of magnetic fields on the quark gluon plasma. Nucl. Phys. A **931**, 752 (2014)

25. U. Gursoy, D. Kharzeev, K. Rajagopal, Magnetohydrodynamics, charged currents and directed flow in heavy ion collisions. Phys. Rev. C **89**(5), 054905 (2014)

26. H. Li, X.-L. Sheng, Q. Wang, Electromagnetic fields with electric and chiral magnetic conductivities in heavy ion collisions. Phys. Rev. C **94**, 044903 (2016)

27. J.P. Goedbloed, R. Keppens, S. Poedts, *Advanced Magnetohydrodynamics with Applications to Laboratory and Astrophysical Plasmas* (Cambridge University Press, 2010)

28. V. Voronyuk et al., Electromagnetic field evolution in relativistic heavy-ion collisions. Phys. Rev. C **83**, 054911 (2011)

29. V. Roy, S. Pu, L. Rezzolla, D.H. Rischke, Analytic Bjorken flow in one-dimensional relativistic magne- tohydrodynamics. Phys. Lett. B **750**, 45 (2015)

30. S. Pu, V. Roy, L. Rezzolla, D.H. Rischke, Bjorken flow in one-dimensional relativistic magnetohydrody- namics with magnetization. Phys. Rev. D **93**, 074022 (2016)

31. S. Pu, Di.-L. Yang, Transverse flow induced by inhomogeneous magnetic fields in the Bjorken expansion. Phys. Rev. D **93**, 054042 (2016)

32. M. Shokri, N. Sadooghi, Evolution of magnetic fields in a transversely expanding highly conductive fluid. JHEP **11**, 181 (2018)

33. I. Siddique, R.J. Wang, S. Pu, Q. Wang, Anomalous magnetohydrodynamics with longitudinal boost invariance and chiral magnetic effect. Phys. Rev. D **99**, 114029 (2019)

34. J.D. Bjorken, Highly relativistic nucleus–nucleus collisions: the central rapidity region. Phys. Rev. D **27**, 140 (1983)

35. T. Csorgo, M.I. Nagy, M. Csanad, A new family of simple solutions of relativistic perfect fluid Hydrody- namics. Phys. Lett. B **663**, 306 (2008)

36. S.S. Gubser, Symmetry constraints on generalizations of Bjorken flow. Phys. Rev. D **82**, 085027 (2010)

37. D. She, Z.F. Jiang, D. Hou, C.B. Yang, 1 + 1 dimensional relativistic magnetohydrodynamics with longitudinal acceleration. Phys. Rev. D **100**, 116014 (2019)

38. G. Inghirami, L. Del Zanna, A. Beraudo, M.H. Moghaddam, F. Becattini, M. Bleicher, Numerical magneto- hydrodynamics for relativistic nuclear collisions. Eur. Phys. J. C **76**, 659 (2016)

39. A. Das, S.S. Dave, P.S. Saumia, A.M. Srivastava, Effects of magnetic field on the plasma evolution in relativistic heavy-ion collisions. Phys. Rev. C **96**, 034902 (2017)

40. S.K. Das, S. Plumari, S. Chatterjee, J. Alam, F. Scardina, V. Greco, Directed flow of charm quarks as a witness of the initial strong magnetic field in ultra-relativistic heavy ion collisions. Phys. Lett. B **768**, 260 (2017)

41. U. Gursoy, D. Kharzeev, E. Marcus, K. Rajagopal, Chun Shen, Charge-dependent flow induced by mag- netic and electric fields in heavy ion collisions. Phys. Rev. C **98**, 055201 (2018)

42. M.I. Nagy, T. Csorgo, M. Csanad, Detailed description of accelerating, simple solutions of relativistic perfect fluid hydrodynamics. Phys. Rev. C **77**, 024908 (2008)

43. K. Adcox et al., [PHENIX Collaboration], Formation of dense partonic matter in relativistic nucleus– nucleus collisions at RHIC: experimental evaluation by the PHENIX Collaboration. Nucl. Phys. A **757**, 184 (2005)